SWAMP SCIENTIFIC REPORT - GROUP C

FIELD SPECTROSCOPY

Jolien Verhelst[1], Elias Berra[2], Yonguang Zhang[3], Conor Cahalane[4], Tommasso Julitta[5]

1. University of Antwerp, Department of Bioscience Engineering, Antwerp, Belgium; jolien.verhelst@uantwerpen.be
2. University of Newcastle, Department of Geomatics, Newcastle upon Tyne, UK; e.f.berra@newcastle.ac.uk
3. Helmholtz Center Potsdam, GFZ German Research Center for Geosciences, Remote Sensing Section, Telegrafenberg A17, 14473 Potsdam, Germany
4. National Centre for Geocomputation, Maynooth University, Co. Kildare, Ireland.
5. Remote Sensing of Environmental Dynamics Lab., DISAT, Università di Milano-Bicocca, P.zza della Scienza 1, 20126 Milano, Italy

1. INTRODUCTION AND AIM OF THE EXPERIMENTS

Bio-monitoring of natural vegetation enables the acquisition of well-defined samples at an affordable cost and allows determining the response of vegetation to environmental changes at different time-scales. It is well known that optical proximal sensing data allow the monitoring of the temporal and spatial variability of biochemical and biophysical plant properties under natural conditions. Optical sensors such as spectroradiometers have been shown to be suitable for the characterization of plant physiological status providing detailed optical characterization of the analysed targets, nevertheless the systems have to be accurately characterized in terms of spectral and radiometric performances in order to obtain repeatable and comparable measurements (Julitta 2015).

Monitoring plant photosynthesis from optical sensors is one of the major interests for remote sensing (RS) in recent years. Since photosynthesis is driven by a wide array of plant-specific and environmental factors, these factors will also induce an effect on the Chlorophyll (Chl) fluorescence signal. The Chl fluorescence signal therefore provides insight into the ability of a plant to tolerate environmental stresses and into the extent to which those stresses have damaged the photosynthetic apparatus (Maxwell and Johnson, 2000). Some examples of physiological stresses which has been studied are water stress (Bukhov et al., 1989), exhaust gases (Makrai et al., 1995), elevated CO_2 (Campbell et al., 2008), and ozone (O_3) fumigation (Calatayud et al., 2002; Gielen et al., 2007; Lorenzini et al., 1999; Meroni et al., 2008a; Meroni et al., 2008b).

Active Chl fluorescence measurements methods make use of an artificial light source. In laboratory conditions, the pulse amplitude modulation (PAM) fluorometry in conjunction with saturation pulse method is often used (Schreiber et al., 1986). Passive Chl fluorescence makes use of the sun's radiation as illumination and excitation source. Chl fluorescence of vegetation represents only 1-5% of the reflected radiance in the near-infrared. The background reflected radiation is therefore much higher compared to the fluorescence signal. This makes the retrieval of fluorescence (Fs) using passive optical remote sensing a challenge. The detection of Fs requires very high resolution spectrometers and the impact of the atmospheric effects needs to be taken into account (Cogliati et al. 2012).

Sun-induced chlorophyll fluorescence (SIF) represents a key optical signal strictly linked to the photosynthetic activity of plants. The analysis of Fs together with spectral indexes related to plant greenness and status such as the widely used Normalized Difference Vegetation Index (NDVI), the Enhanced Vegetation Index (EVI) and the Photochemical Reflectance Index (PRI) can provide detailed information about plant photosynthesis (Cogliati et al. 2012).

The aim of this work was to infer and map the spatial patterns of the productivity from fluorescence and reflectance for a wetland site. It was also attempted to calibrate and validate a SCOPE model. Ultimately, the measurements of fluorescence could be used to validate APEX, HyPlant, UAV and Sentinel 2a sensors.

2 TEST SITE AND COLLABORATIONS

This EUFAR/OPTIMISE funded study was carried out at Obrzycko-Rzecin, Poland from July 6th to 16th, 2015. It was designed to combine data from a number of aerial and terrestrial survey platforms.

The following sections detail the test site, the survey hardware and the collaborations involved in this portion of the field measurements.

2.1 Test Site - POWLWET

POLWET is a semi-natural wetland located near Obrzycko-Rzecin, Poland (Figure 1a). It offers facilities for eddy-covariance measurements and also automatic chamber measurements of CH_4 and N_2O flux measurements. It is regularly used for measurement campaigns, incorporates weather stations and offers AC and DC power supplies. The tests performed by Group C during this study would be the first to measure fluorescence using field spectrometers in a wetland. A boardwalk running throughout the test site to the chambers and flux tower would enable measurements to be taken at specific locations along the area (Figure 1b).

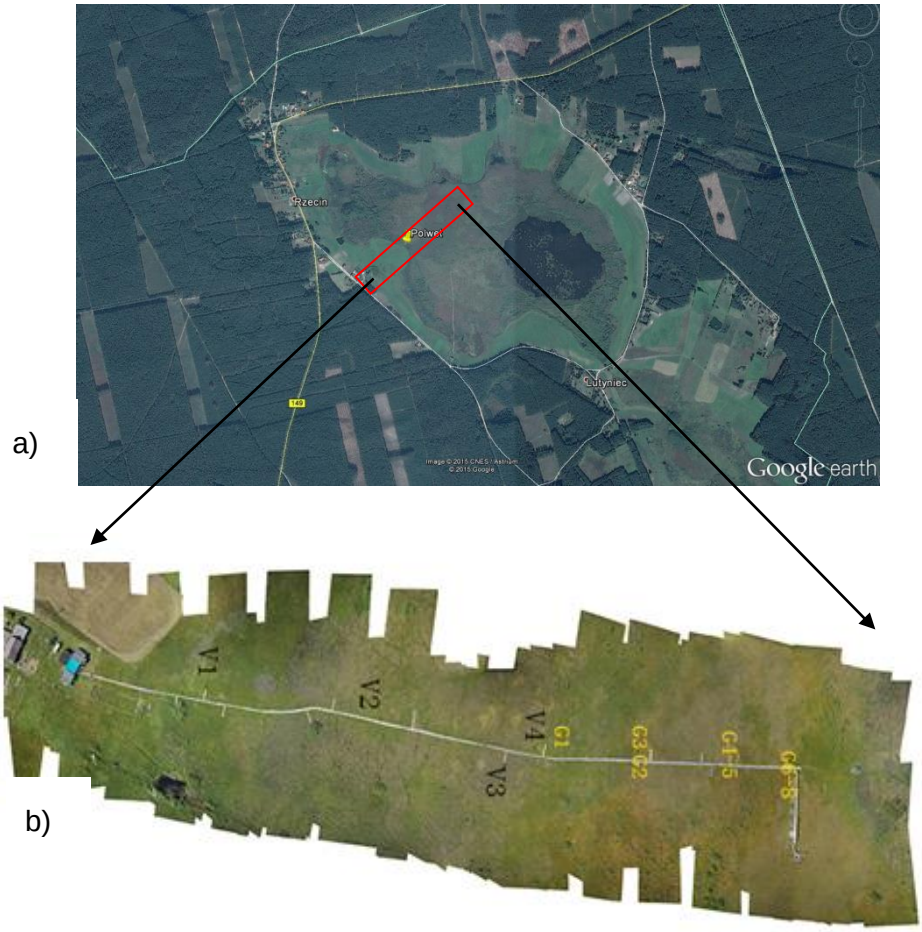

Figure 1: General overview of the POLWET station (a). A detailed UAV-derived orthomosaic showing the boardwalk and the sampling units locations where spectro-radiometric and chamber gas measurements were taken (b).

2.2 Flight Preparation and Flight Planning

One of the primary components of this study was to plan, and conduct airborne research in conjunction with a (near-) ground measurement campaign. Consequently a flight-plan was prepared in conjunction with other participants. Two aerial platforms operating hyperspectral sensors were scheduled for an overpass on the survey dates, APEX and HyPlant, however due to issues with cloud cover and flying regulations APEX was not employed initially.

The flight plan was designed to ensure the central flight line would cross the wetland boardwalk (Figure 1) at nadir view. The spatial resolution of the imagery would be 1.2 m at the lowest permissible flying height. A series of bright and dark canvas targets were positioned in the test are to assist in atmospheric correction and converting the at-sensor radiance values to absolute surface reflectance. As blue-skies are required for accurate spectral measurements, a number of delays were encountered waiting for a suitable weather window.

2.3 UAV Measurements

A number of UAVs providing near-ground spectral measurements operated in conjunction with the field and airborne campaigns. These were a Falcon 8 OctoCopter from AscTec, with an adapted Ocean Optics spectrometer collecting BRDF measurements. The camera gimble enables hemispherical measurements over points of interest. A second, bespoke UAV operating a Rikola Hyperspectral Imager (a Fabry-Perot Interferometer) was also operating in the test area. The results from the field campaign could be combined with the UAV data in future work.

2.4 Group C Field Measurements

Simultaneously, the grass radiances were measured with an automatic system named S-FLUO box. The S-FLUO box system hosts two portable spectrometers (HR4000, Ocean Optics, USA) characterized by different spectral resolutions. One sensor measures the 'full' spectrum from 350nm to 1050nm at a 1 nm spectral resolution (Full width at Hal Maximum, FWHM) and another measuring a narrow band from 650nm to 840nm with 0.2 nm of spectral resolution (FWHM) (Table 1). As the sensors required the thermally cooled housing and a generator to power it, care had to be taken when operating near the flux tower.

Table 1: Spectrometers characteristics.

Spectrometer	FWHM (nm)	Sampling interval (nm)	Spectral range (nm)	Application
Spec 1	1	0.24	350-1050	Irrad. measurements, ρ and VIs computation
Spec 2	0.2	0.05	650-840	Sun-induced Chl fluorescence at O_2-A

Fibre optics carry the spectral measurements from the end of the tripod arm to the two sensors contained in a thermally cooled case (Figure 2) and enable precise field measurements. A graduated tripod enables angular precision for repeat measurements. The dark current cover at the end of the measurement arm enables noise during the measurement process to be measured.

Figure 2: Portable spectrometers used to measure radiance over the POLWET plots (Figure 1).

2.5 Collaborations

The fluorescence measurements recorded by Group C in the field campaign would be essential for a number of other measurement campaigns in progress simultaneously. Close cooperation was required with Group D to agree on measurement locations for their leaf clip measurements as top of canopy fluorescence was required. Collaboration between the field measurement campaign and the UAV teams was also required. The positions of each measurement were agreed upon in the measurement planning stages and the measurement locations were recorded with single frequency GPS following the tests and provided to each group. An additional series of tests were designed to run in conjunction with a Polish survey team, whereby manual gas chamber measurements were recorded after the Spectroscopy team moved on to the subsequent points.

3. METHODOLOGY

Early survey planning discussions resulted in a series of 4 vegetation sites and 8 gas chamber sites being selected for the field campaign. Figure 1(b) displays the measurement locations in the test area for the field spectroscopy team. Two alternatives methodologies were presented by the field team, and these would depend on whether a second overpass was performed by the aerial platforms. Ultimately, a second overpass was performed and therefore a second series of measurements were recorded. The following sections discuss the methodology employed in the field campaign.

3.1 Vegetation measurements

POLWET contains unique vegetation species adapted for wet environments (Figure 3a-d). Five vegetation locations (Figure 1b), V1-V5 were selected during the mission planning stage. These were given priority to coincide with the airborne flyovers. Two series of measurements were recorded - Series 1 coincided with the first HyPlant overpass and Series 2 with the second. Five measurements over each plot were recorded and then linearly averaged to reduce noise in the sample. Each measurement cycle consisted of four spectra: first, a measurement of the dark current followed by 3 spectra whereby a measurement of the target's up-welling radiance was sandwiched between two solar irradiance measurements (e.g., dark current, irradiance, target, irradiance). The solar irradiance at the time of the target measurement was estimated by linear interpolation over the cycle's 1 minute duration.

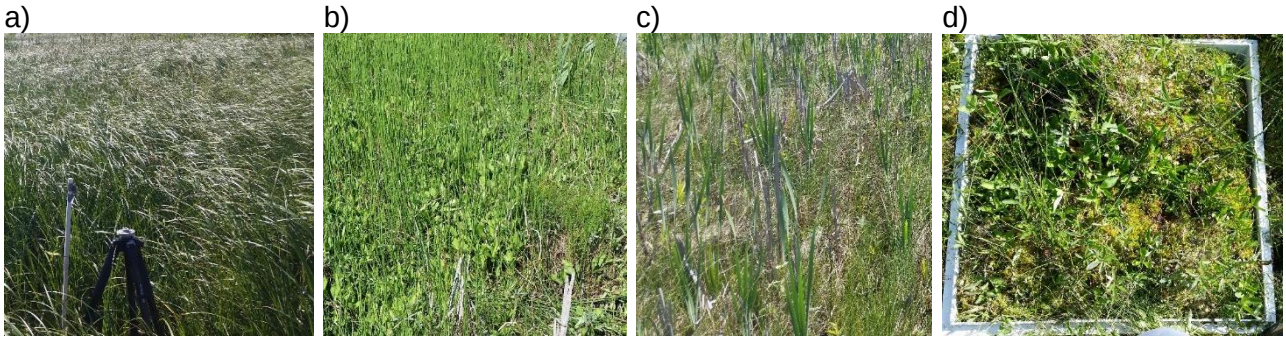

Figure 3: Photographs of natural vegetation common found at POLWET station from which spectral measurements were collected. The photographs represent the locations V1 (a), V2 (b), V3 (c) and V4 (d) according to Figure 1.

3.2 Gas Chamber Measurements

Due to time constraints five chamber locations were selected from the original eight (Figure 1b). To maximise the value of these measurements 5 different types of sample (Figure 4a) were selected. Only a single series of measurements were performed during the gas chamber stage of the measurement campaign. Again, a combination of dark current measurements, white reference panel measurements and sample measurements to minimise noise in post-processing and increase the

reliability of sample measurements. These measurements were performed in collaboration with the gas chamber team (Figure 4b).

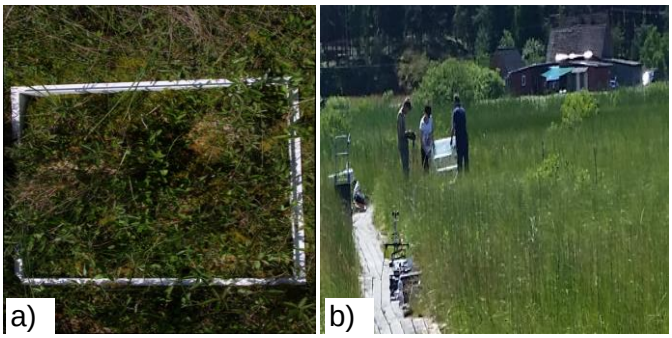

Figure 4: (a) Wetland vegetation sample from which both radiometric and gas chamber measurements were taken. (b) Team carrying out gas chamber measurements.

3.3 Measurement Issues

Performing the measurement campaign with the field spectrometer was a laborious process in the confined surroundings of the boardwalk. The sensitive nature of the surrounding environment and the large numbers of people operating simultaneously in the survey area minimised the options for placing the survey equipment. A number of issues lead to delays in the survey campaign:

- A constant power supply (the generator) resulted in an extensive network of cables cluttering the survey area and required transport to each test location.
- The generator could not be located in the vicinity of the flux tower.
- A shortage of fuel during the tests lead to an increase in the temperature in the thermally cooled box potentially introducing errors (noted in metadata).
- Damage to one of the tripods required repair before measurements could recommence.

3.4 Data Processing and Analysis

A number of processing stages were required during the spectral calibration of raw data. A general procedure for data processing to obtain radiance value and reflectance factor is given accordingly (Julitta 2015):

1. *Correction for temperature variability*. The temperature dependency of the measurement needs to be known from laboratory test in order to correct the signal. A trace back of the temperature measurements has to be collected.
2. *Correction for dark current*. The dark current signal collected with the same integration time has to be subtracted from the spectrum.
3. *Nonlinearity correction*. The nonlinearity laboratory characterization has to be applied to reduce the measurement uncertainty. Is generally suggested to avoid optimizing the signal in the higher part of the spectrum (80%).
4. *Wavelength correction*. Wavelength corrections gains need to be applied to compensate for the spectral shift of the detector.
5. *Radiometric calibration*. In order to obtain a measurement expressed in a physical unit the previously calculated radiometric coefficients have to be applied.
6. *Calculation of the reference value at the measurement time*. This step refers to a single beam device. To overcome the problem related to different time acquisition of reference and target the reference value has to be referred at the target acquisition times using a linear interpolation between the two references.

The above steps assure calibrated radiance can be calculated, which values were used to calculate fluorescence, reflectance and reflectance-derived vegetation indices.

Sun-induced chlorophyll fluorescence (SIF) was calculated as follows (Plascyk 1975):

$$F = \frac{E\lambda out \times L\lambda in - L\lambda out \times E\lambda in}{E\lambda ou - E\lambda in}$$

Where E is the incident solar irradiance and L is the target radiance. λin and λout refer to the wavelengths at the bottoms and at the shoulders of the absorption features, respectively.

Reflectance factor (R) computation is calculated as follows bellow (Julitta 2015), which values were thereafter used to calculate four vegetation index as shown in Table2:

$$R = \frac{\pi * L_{Down\_radiance}}{E_{Up\_irradiance}}$$

Where down radiance $L_{Down\_radiance}$ is reflected radiance (unit: w·m-2·nm-1·sr-1), and $E_{Up\_irradiance}$ is the incoming irradiance (unit: w·m-2·nm-1).

Table 2: Vegetation indices used in this study: Normalized Difference Vegetation Index (NDVI), Enhanced Vegetation Index (EVI), MERIS Terrestrial Chlorophyll Index (MTCI) and Photochemical Reflectance Index (PRI). R indicates reflectance and numbers indicate wavelength in nanometres at the centre of the bands.

Index	Formulation	Reference
NDVI	$\frac{R865 - R655}{R865 + R655}$	Rouse et al (1973)
EVI		
MTCI	$\frac{R753.75 - R708.75}{R708.75 - R681}$	Dash and Curran (2004)
PRI	$\frac{R531 - R570}{R531 + R570}$	(Gamon et al, 1992)

3.5 Meta Data Creation and Online Spectral Database (SPECCHIO)

An additional component of the survey campaign was to combine all survey data in a central location and standardise the metadata across the separate survey groups. SPECCHIO - a spectral information system (http://www.specchio.ch/) was employed for this purpose. The binary files were incompatible with SPECCHIO however a csv reader was developed by the developer to store the information from the HR4000. Additional information for each test site, including station description sites, photographs and raw data were uploaded to SPECCHIO.

4. RESULTS

The reflected spectral radiance, as measured with the higher spectral resolution spectrometer, (Spec 2, Table 1) shows a peak of reflectance cantered at 760 nm (Figure 5a) which can be associated with emission of fluorescence (Julitta 2015). There can also be observed peaks of reflectance in all samples, although exhibiting different intensities. It can be noticed that the different series (S1 and S2) have similar shape but different intensities, presumably is due to diffuclties involved in replicate the same environmental and geometry conditions for each measurement.

Figure 6 shows the fluorescence values retrieved from the HR4000 spectrometers. Higher peaks of reflectance at around 760 nm are generally associated with higher emission of fluorescence. For example, V1 plot has the highest peak amongst the samples (Figure 5a), which in turn makes V1 have the highest emission of fluorescence (Figure 6a). On the contrary, lower reflectance peaks tend to be associated with lower fluorescence values.

Different times of observation (S1 and S2) resulted in different fluorescence intensities (Figure 6), which is in agreement with observations of reflectance over the same plots (Figure 5). A factor contributing to this can be the different solar zenith angles during the two series of measurements.

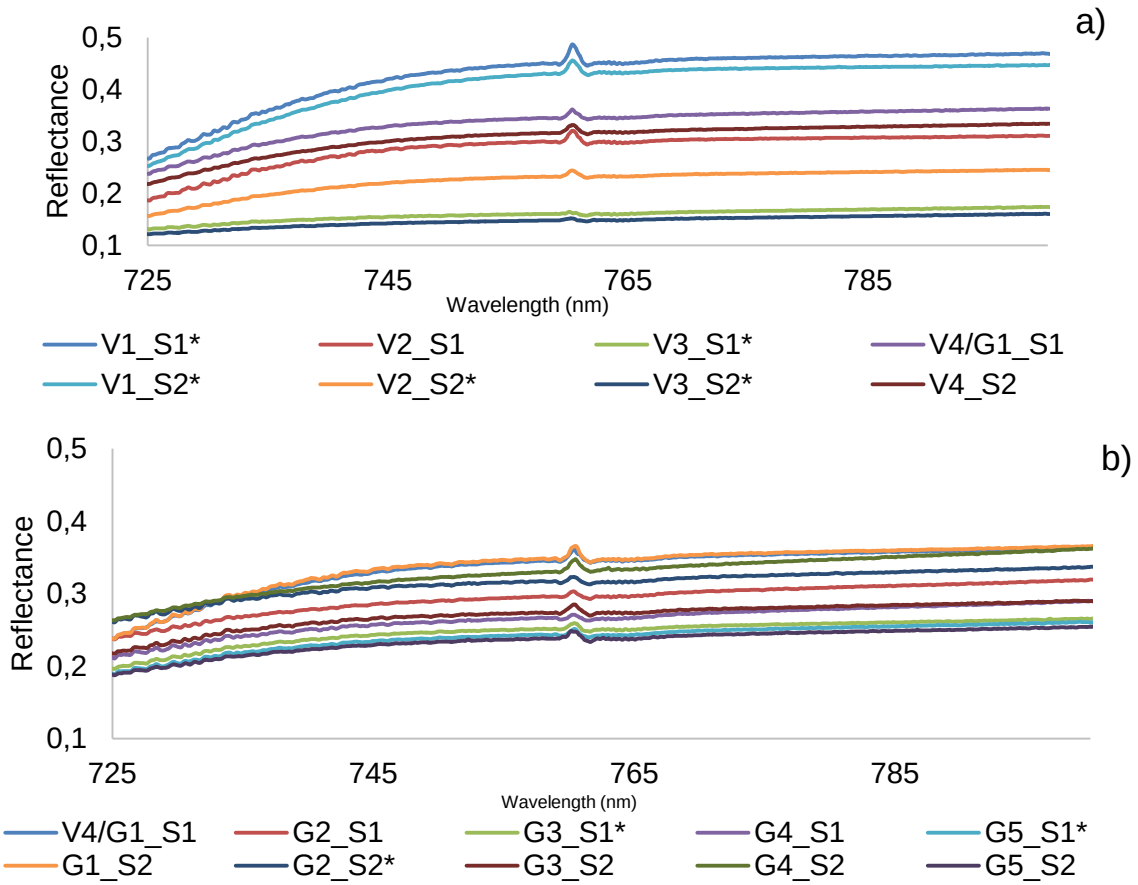

Figure 5: Apparent reflectance from vegetation (a) and chambers plots (b) measured with high spectral resolution radiometer. S1 stands for the first series of measurements and S2 for the second one.

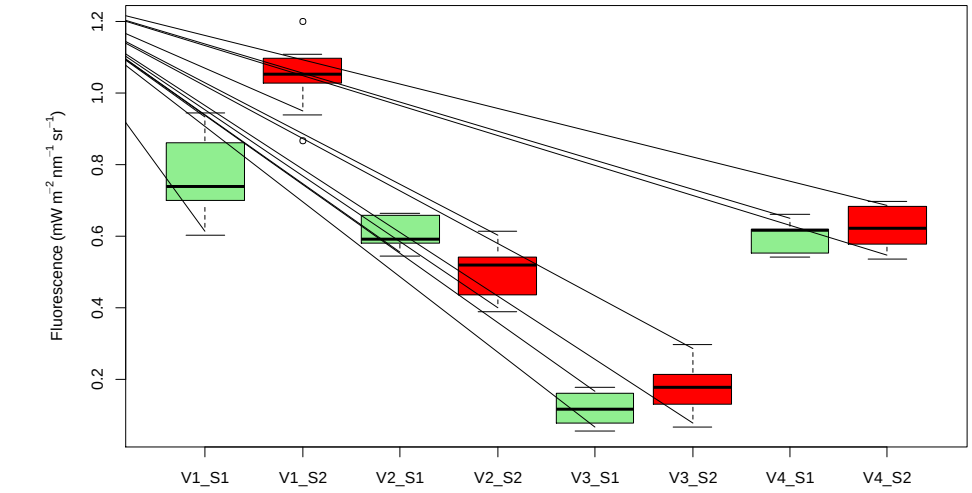

a)

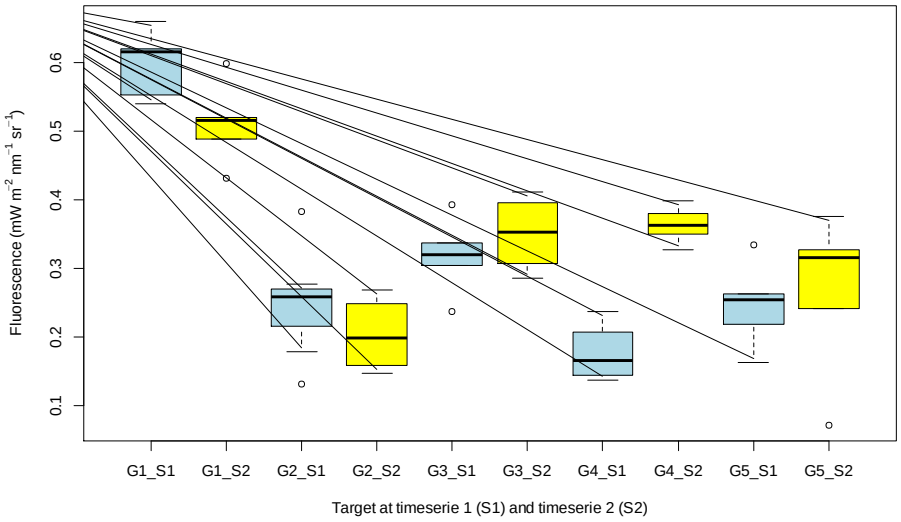

b)

Figure 6: Boxplots of SIF measured at times S1 and S2 over vegetation plots (V) (a) and chamber (G) plots (b).

Figure 7 shows empirical relationship between spectral vegetation indices and SFI. EVI has had the strongest agreement with SFI (R^2=0.82), while NDVI and MTCI had similar R^2, 0.73 and 0.74, respectively. PRI, EVI*cos(SZA) and NPQI explain poorly the SFI variance. It can be also seen that EVI and MTCI have linear relationship with fluorescence, but NDVI has a nonlinear relationship which points out saturation issues of this index.

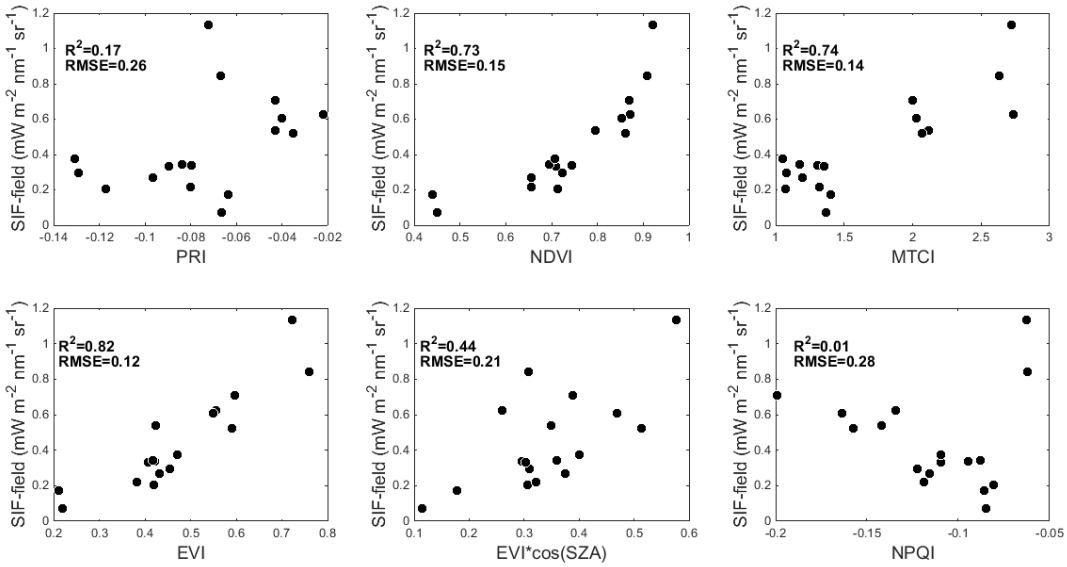

*Figure 7: Relationships between spectral vegetation indices PRI, NDVI, MTCI, EVI, EVI*cos(SZA) and solar induced fluorescence (SIF), for a wetland vegetation.*

4.3 The Scope Model

We carried out the simulations for all the plots using SCOPE to model photosynthesis and fluorescence at both leaf and canopy level. SCOPE is a vertical (1-D) schematization of the vegetation that simulates radiative transfer and the exchange of heat, CO2 and H2 O between soil, vegetation and the atmosphere. The reflectance and transmittance of the leaf are calculated with the module Fluspect, which is an extension of the PROSPECT model (Jacquemoud et al., 2009). The extension consists of the calculation of the scattering of chlorophyll fluorescence within the leaf. The radiative transfer of incident (solar and sky) light through the canopy is calculated with the SAIL model (Verhoef , 1984) in which 60 elementary layers, 13 leaf zenith and 36 leaf azimuth classes are distinguished. The incident light on each leaf is further used to compute the internally generated radiation per leaf layer and leaf inclination class: thermal radiation (using Planck's law) and chlorophyll fluorescence (using Fluspect). The radiative transfer of these internally generated fluxes through the canopy is calculated with a module similar to the FluorSAIL model (Miller et al., 2005), but contrary to the FluorSAIL model, SCOPE uses a numerical solution that allows each class to have a different emission (van der Tol et al., 2009b).

An input of the radiative transfer modules is the fluorescence emission efficiency ε, which is the probability that an absorbed photon in the photosynthetically active region of the spectrum (PAR), is re-emitted as fluorescence. A constant ε implies that the simulated SIF is exactly proportional to APAR. In SCOPE it is assumed that ε of photosystem I (PS-I) is constant, and hence, the SIF produced by PS-I is proportional to APAR. The emission efficiency of PS-II is not kept constant, but it is calculated with a semi-empirical model for photosynthesis and fluorescence emission based on leaf-level measurements of gas exchange and active fluorescence measurement techniques. Originally, the model of van der Tol et al. (2009b) was used, but in the version used in the version used in the present paper, the model of van der Tol et al. (2014) has been used. This model simulates the fate of absorbed photons, which has three dissipation pathways: photochemical quenching (PQ), non-

photochemical quenching (NPQ), and fluorescence. The probabilities are calculated with rate coefficients K with subscripts f for fluorescence, pq for photochemical quenching and npq for non-photochemical quenching:

$$\varepsilon \propto \frac{K_f}{K_f + K_{pq} + K_{npq}} \quad (1)$$

Kf is a constant, but Kpq and Knpq both vary. Kpq varies because the efficiency of photochemical use of photons depends on the capacity of the photosystems to transport electrons, while Knpq varies because of quickly reversible protective mechanisms that enable the dissipation of excess energy. In the model of van der Tol et al. (2014), two alternative empirical calibrations of Knpq are available. The model contains two empirical fits of for Knpq . Here we use a parameterization calibrated to outdoor measurements of Flexas et al. (2002) on plants under variable drought conditions as a function of the light saturation of photosynthesis x:

$$K_{npq} = \nu K_n^o \quad \text{with} \quad \nu = \frac{(1+\beta)x^\alpha}{\beta + x^\alpha} \quad (2)$$

where $\mathbf{K_n^o}$, α and β are fitting parameters with values $\mathbf{K_n^o}$ = 5.01, α = 1.93 and β = 10. The variable x is crucial, it is the ratio of actual over potential (ligth limited) photochemistry, and it is calculated from the photosynthesis model. The variability of ε for PS-II is responsible for the fact that SIF is not always proportional to NPQ. Its value is calculated from x, which in turn depends on the carboxylation capacity Vcmax , the irradiance on the leaf, stomatal aperture and leaf temperature. An updated version of the SCOPE model was used here (v1.60). More details can be referred in van der Tol et al. (2009b, 2014).

The input parameters for SCOPE include meteorological forcing (incoming shortwave and long-wave radiation, air temperature and pressure, humidity, wind speed, and CO2 concentration), LAI, leaf angle distribution, leaf chlorophyll content (Cab), stomatal conductance parameter (m), and maximum carboxylation capacity, Vcmax. Meteorological inputs were available from the SWAMP flux site measurements. An estimation of Cab, Cw, Cdm, N, LIDa, and LIDb controlling the leaf and canopy radiative transfer was obtained from the reflectance measurements. We use an optimization approach to solve the inversion problem. The leaf reflectance model PROSPECT (Jacquemoud and Baret, 1990) was used for the inversion, which was also integrated into the SCOPE model. A simple cost function was used to find the solution to the inverse problem, which minimizes the root mean squared error (RMSE) between measured and simulated reflectance spectrum. The resulting variables of these parameters were used as input biophysical parameters for SCOPE at each plot.

4.4 Future Work

A number of potential avenues can be investigated for future work. Excluding further interrogation of the results from the Ocean Optics survey of the vegetation surveys - four other datasets could be included for comparison:

- APEX data: Due to problems with flight regulations the APEX hyperpectral imagery was not captured on the day of the field survey. A subsequent flight later in the month was carried out and data can be requested from EUFAR for these purposes.

- Rikkola data: The Rikkola fabry-perot interferometer had recorded hyperspectral imagery for a number of the test sites. GPS coordinates for each sample location have been recorded and stored in SPECCHIO with other metadata for the survey campaign. These can be compared with the low-altitude airborne imagery.

- Satellite data: A Sentinel 2a overpass was scheduled for that day. Although Sentinel 2a is multispectral rather than hyperspectral and although the data has not been fully calibrated, this would be an interesting comparison. The field measurements could potentially feed into a validation component for the Sentinel missions.

- Gas chambers: Comparisons with chamber measurements recorded by Polish field survey team and field measurements recorded by SWAMP members can also form a component of future work.

5. CONCLUSIONS

The SWAMP project was an ambitious undertaking, combining a number of field survey groups, low flying UAVs, mid-altitude Hyperspectral fixed wing aircraft and new ESA satellites. Despite issues with logistics on the day of the survey the field spectroscopy group (Group C) recorded measurements for a number of locations, including vegetation plots and gas chamber sites and through careful mission planning were able to schedule these surveys to coincide with two aerial overpasses of the HyPlant aircraft, maximising the value of the data for future studies. This is the first time that fluorescence was measured successfully in this wetland and the data has been made available for all interested parties in the OPTIMISE spectral information system, SPECCHIO. NDVIs are known to show saturation, and the relationship recorded in this field campaign by Group C with fluorescence indicates that far-red SIF is not saturating, therefore adding some useful information when compared only to a traditional index such as NDVI. This data (particularly SIF) will then be particularly useful in further calibration of other datasets, such as HyPlant and APEX. Additional comparisons with the SCOPE model has demonstrated that the simulations can be constrained with the field data but also can be constrained with the spectral data. Future work can include comparisons with airborne hyperspectral data, gas chamber measurements or aiding with Sentinel 2 multispectral calibration.

ACKNOWLEDGEMENTS

"The research leading to these results has received funding from the European Community's Seventh Framework Programme (*FP7/2014-2018*) under *grant agreement* n°312609 (EUFAR: European Facility for Airborne Research in Environmental and Geo-sciences), COST Action ES1309 OPTIMISE (Innovative Optical Tools for Proximal Sensing of Ecophysiological Processes and the European Space Agency.

REFERENCES

Maxwell K and Johnson G N (2000) Chlorophyll fluorescence - a practical guide. Journal of experimental botany, Vol. 51/345, 659 – 668.

Zarco-Tejada P J, Miller J R, Mohammed G H, Noland T L and Sampson P H (2000) Chlorophyll fluorescence effects on vegetation apparent reflectance: II. Laboratory and airborne canopy-level measurements with hyperspectral data. Remote Sensing of Environment 74, 596-608.

Bukhov, N G, Sabat, S C, Mohanty, P (1989) Sequential loss of photosynthetic functions during leaf desiccation as monitored by Chl fluorescence transient. Plant Cell Physiology 30, 393-398.

Makrai L, Dulai S and Lehoczki E (1995) The photosynthetic performance of oak populations exposed to automobile exhaust as an air pollutant. Photosynthesis: from light to biosphere Vol. V, 993-996.

Campbell P K E, Middleton E M, Corp L A, Kim, M S (2008) Contribution of chlorophyll fluorescence to the apparent vegetation reflectance. Science of the Total Environment 404, 433-439.

Calatayud A, Ramirez J W, Iglesias D J, Barreno E (2002) Effects of ozone on photosynthetic CO2 exchange, chlorophyll a fluorescence and antioxidant systems in lettuce leaves. Physiologia Plantarum 116, 308-316.

Cogliati, S., Colombo, R., Rossini, M., Meroni, M., Julitta, T., & Panigada, C. (2012). Retrieval of vegetation fluorescence from ground-based and airborne high resolution measurements. In, *Geoscience and Remote Sensing Symposium (IGARSS), 2012 IEEE International* (pp. 7129-7132): IEEE

Gamon, J.A., Peñuelas, J., Field, C.B., 1992. A narrow-waveband spectral index that tracks diurnal changes in photosynthetic efficiency. Remote Sens. Environ. 41, 35–44.

Gielen B, Löw M, Deckmyn G, Metzger U, Franck F, Heerdt C, Matyssek R, Valcke R, Ceulemans R (2007) Chronic ozone exposure affects leaf senescence of adult beech trees: a chlorophyll fluorescence approach. Journal of Experimental Botany 58, 785-795.

Julitta, T. (2015). Optical proximal sensing for vegetation monitoring. In, *Faculty of Mathematical, Physical and Natural Sciences, Department of Environmental and Earth Sciences, University of Milano-Bicocca, Milan, Italy* (p. 136): University of Milano-Bicocca, Milan, Italy

Lorenzini G, Guidi L, Nali C, Franco G (1999) Quenching analysis in poplar clones exposed to ozone. Tree Physiology 19, 607-612.

Meroni M, Picchi V, Rossini M, Cogliati S, Panigada C, Nali C, Lorenzini G, Colombo R (2008a) Leaf level early assessment of ozone injuries by passive fluorescence and photochemical reflectance index. International Journal of Remote Sensing 29, 5409-5422.

Meroni M, Rossini M, Picchi V, Panigada C, Cogliati S, Nali C, Colombo R (2008b) Assessing steady-state fluorescence and PRI from hyperspectral proximal sensing as early indicators of plant stress: The case of ozone exposure. Sensors 8, 1740-1754.

Plascyk, J. A. The MK II Fraunhofer Line Discriminator /FLD-II/ for airborne and orbital remote sensing of solar-stimulated luminescence. Opt. Eng. 1975, 14, 339–346.

Schreiber U, Schliwa U, Bilger W (1986) Continuous recording of photochemical and non-photochemical chlorophyll fluorescence quenching with a new type of modulation fluoreometer. Photosynthesis research 10, 51-62.

van der Tol, C., W. Verhoef, and A. Rosema (2009a), A model for chlorophyll fluorescence and photosynthesis at leaf scale, Agricultural and Forest Meteorology, 149(1), 96 - 105.

van der Tol, C., W. Verhoef, J. Timmermans, A. Verhoef, and Z. Su (2009b), An integrated model of soil-canopy spectral radiances, photosynthesis, fluorescence, temperature and energy balance, Biogeosciences, 6, 3109-3129.

van der Tol, C., J. Berry, P. Campbell, and U. Rascher (2014), Models of fluorescence and photosynthesis for interpreting measurements of solar-induced chlorophyll fluorescence, Journal of Geophysical Research: Biogeosciences, 119(12), 2312-2327.

Verhoef, W. (1984), Light scattering by leaf layers with application to canopy reflectance modeling: the sail model, Remote sensing of environment, 16(2), 125-141.